Journal of Materials Chemistry C

Accepted Manuscript

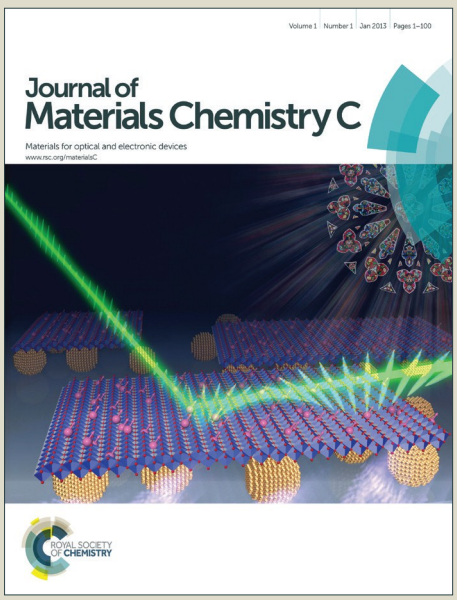

ROYAL SOCIETY OF CHEMISTRY

www.rsc.org/materialsC

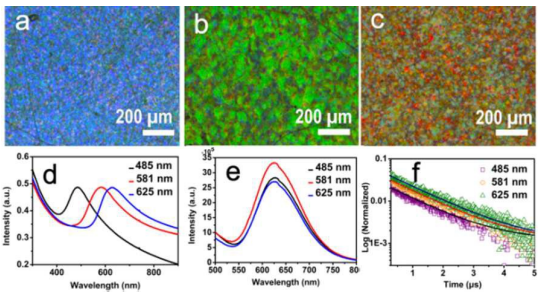

AuNC-CNC films demonstrate modulated fluorescence emission and lifetime decay due to the photonic crystal-photoemission coupling effect.

Journal Name

COMMUNICATION

Chiral fluorescent films of gold nanocluster and photonic cellulose with modulated fluorescence emission

Received 00th January 20xx,
Accepted 00th January 20xx

DOI: 10.1039/x0xx00000x

www.rsc.org/

Dan Qu,[a] Jianan Zhang,[b] Guang Chu,[a] Haijing Jiang,[a] Changfeng Wu*[b] and Yan Xu*[a]

Chiral fluorescent composite films of gold nanoclusters (AuNC) and photonic cellulose nanocrystals (CNC) demonstrate modulated fluorescence emission due to the stopband- and band edge-photoemission coupling effect between the photonic CNC and fluorescent AuNC , showing promising potentials as fluorescent nanosensors, optical switches and optical memory devices.

The design and fabrication of chiral nematic materials with chiroptical-modulated properties may lead to a new generation of smart materials, sensors, and imaging and labelling tools.[1] Cellulose is the most abundant renewable biopolymer on earth. In nature, the solid-state chiral nematic organization of cellulose in plant cell walls gives rise to the brilliant iridescent colours of marble berries and tropical leafs.[2] Integrating the opto-electronic properties of chiral nematic host structures with stimuli-responsive guest species may afford new chiral nematic materials with an advanced set of functions.[3]

CNC, when charged, may self-assemble into a stable chiral nematic structure that can be preserved upon drying, giving rise to iridescent films with visible iridescent colours when the helical pitch is in the order of the wavelength of visible light.[4] Chiral nematic CNC has been a much attended topic since 2010 due to the discovery that the helical order of CNC can be transferred to solid replica through mineralization and corporative assembly. It opens up new horizons for smart materials with optical responsiveness, and also for optical-based nanosensors and nanoprobes. Chiral nematic CNC has been explored as a template for free-standing chiral nematic mesoporous films of silica and organosilica by mineralization, and chiral nematic mesoporous film of titania by inverse replication.[5] Organizing rare earth species into a chiral nematic structure manifests the possibility of modulating spontaneous emission and circularly polarized excitation as showcased by ZrO_2:Eu^{3+}, Y_2O_3:Eu^{3+} and YVO_4:Eu^{3+}.[6] Integrating noble metal nanoblocks with chiral nematic structure leads to chiral nematic mesoporous films of AgNP-SiO_2, and AuNR-CNC and AuNP-CNC, showing an optical response associated with the chiral assembly of AgNP, and strong plasmonic chiroptical activity, respectively. Alternative view in regards with plasmonic chiroptical activity has been reported.[7] Chiral nematic composite films of AgNW-CNC exhibit strong and tunable chiral plasmonic optical activity, and electromagnetic energy transfer.[8] The factors that influence the structure and properties in latex NP-CNC, and entropically driven coassembly behaviour between latex NP and CNC have been studied.[9] The chiral nematic mesoporous films of CdS-SiO_2 and poly (p-phenylenevinylene) (PPV)-organosilica, encapsulating fluorescent CdS and PPV respectively, show photoemission and chiral nematic order where the modulation of spontaneous emission was not reported.[10] Quantum dots like CdS hold exciting implications for applications like optical switches and fluorescence probes in biological assays due to their unique optical properties such as narrow and size-tunable emission spectrum, high quantum efficiency and strong nonlinear response. However, the intrinsic drawbacks like toxicity and photochemical stability call for new chiral nematic luminescent materials with good optical and chemical stability, and low toxicity.

AuNC is a special class of gold nanomaterials with dimensions smaller than 3 nm.[11] This dimension is comparable to the Fermi wavelength of the conduction electrons. The spatial confinement of free electrons in AuNC results in discrete and size-tunable electronic transitions, leading to molecular-like properties such as luminescence.[12] With the advantages of long lifetime, large Stokes shifts, low cytotoxicity and biocompatibility, AuNC has become important candidates for sensing and bioimaging applications.[13] To the

[a] State Key Laboratory of Inorganic Synthesis and Preparative Chemistry, Jilin University, 2699 Qianjin Street, Changchun 130012, China. E-mail: yanxu@jlu.edu.cn
[b] State Key Laboratory of Integrated Optoelectronics, College of Electronic Science and Engineering, Jilin University, 2699 Qianjin Street, Changchun 130012, China. E-mail: cwu@jlu.edu.cn

‡ Electronic Supplementary Information (ESI) available: details of experimental procedures; Photograph, SEM, TEM, POM, LSCM, UV-vis, CD, fluorescence spectra, tables with analytical data. See DOI: 10.1039/x0xx00000x

best of our knowledge, free-standing chiral nematic CNC films with embedded AuNC have never been reported so far.

Herein, we describe the fabrication of free-standing composite films of AuNC-CNC by a facile evaporation-induced corporative assembly method. Rodlike CNC prepared by sulfuric acid hydrolysis carries negative charges due to imparted sulfate ester groups. To allow tuning of AuNC loading while avoiding flocculation, a repulsion-driven corporative assembly route using hydrophilic and negatively charged AuNC is adopted. For that matter, a bovine serum albumin (BSA) stablized AuNC composed of 25 gold atoms within the scaffold of BSA is used. Free-standing fluorescent and iridescent films of AuNC-CNC containing uniformly distributed AuNC have been obtained. We discover the chiroptical-dependent fluorescence emission of AuNC-CNC in red regime, that the fluorescence lifetime decay can be tuned by the photonic stopband, and the peak intensity be tuned by the stopband- and band edge-photoemission coupling effect. Less than onefold enhancement of fluorescence intensity and ON/OFF ratio have been observed that is in compatible to the reported values by one-dimensional photonic crystals, however, less significant compared with 40-fold and 108-fold enhancement by three- and two-dimensional photonic crystals, respectively.[14] The AuNC-CNC composite films offer alternative choice as free-standing fluorescence sensors, and for imaging and labelling applications.

AuNC was prepared from $HAuCl_4$ using BSA as a reducing and stabilizing agent by a modified procedure based on Yin's work (Experimental in ESI).[13a] The photoemission peak centred at 640 nm confirms the presence of Au_{25} nanocluster (Fig. S1). The average size of AuNC is about 3 nm based on the transmission electron microscopy (TEM) images (Fig. S2a, 2b). The aqueous solution of AuNC is positively charged below the isoelectric point of BSA at pH = 4.7, and negatively charged above the isoelectric point of BSA. The CNC nanorod obtained by sulfuric acid hydrolysis has an average dimension of 10-20 nm in width and 200-300 nm in length based on the TEM imaging analysis (Fig. S2c).[6c] CNC film shows left-handed chiral nematic order (Fig. S2d). The as-prepared CNC suspension is negatively charged. AuNC and CNC may self-organize forming a host-guest composite film via repulsive interactions. The composite film, designated as $AuNC_x$-CNC, was prepared typically by adding x mL of 2.5 mM AuNC solution to 5 mL of 3 wt% CNC suspension with the pH adjusted to 7 to render AuNC negative charges. The ζ-potential of CNCs and AuNC are -51.7 mV and -28.8 mV, respectively. $AuNC_x$-CNC (x = 0, 0.5, 1, 2, 3 and 4) with preserved chiral nematic order has been obtained from stable $AuNC_x$:CNC suspension mixes that show no sign of flocculation during the corporative assembly (Table S1). Taking the suspension mix containing 4.0 mL of AuNC for example, a fingerprint texture and strong birefringence with domains of different orientations are observed by polarized optical microscopy (POM) during and after evaporation, indicating that the addition of AuNC does not disturb the formation of chiral nematic ordering (Fig. S3a, S4).[15] The chiral nematic structure of $AuNC_4$-CNC is further confirmed by high magnification scanning electron microscope (SEM) showing

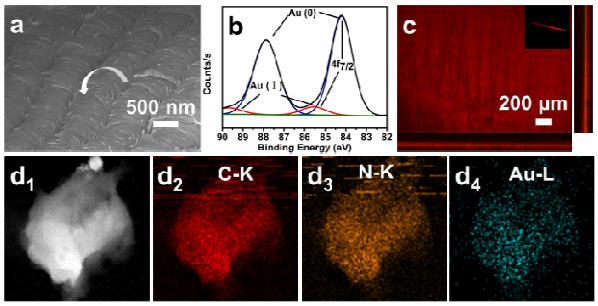

Fig 1. (a) High magnification SEM of $AuNC_4$-CNC showing the periodic arrangement with helical pitch in the order of several hundred nanometers and a left-handed orientation. (b) XPS of $AuNC_4$-CNC showing the presence of Au(0) and Au(I). (c) LSCM images of $AuNC_4$-CNC showing AuNC distribution in the body (main image) and along the side (Inset) of the film. (d_1) HAADF-STEM image and (d_2-d_4) EDX elemental mapping of C, N and Au, showing the uniform distribution of AuNC in $AuNC_4$-CNC.

the periodic and left-handed helical arrangement with the helical pitch in the order of several hundred nanometers (Fig. 1a). Both Au(0) atoms and Au(I) ions are found in $AuNC_4$-CNC based on the deconvoluted X-ray photoelectron spectroscopy (XPS) peaks of Au $4f_{7/2}$ at 84.0 eV and 85.4 eV, respectively, with an approximate ratio of 100:9, where Au(I) ions are believed contributing to the stabilization of AuNC (Fig. 1b).[13a] The distribution of AuNC in $AuNC_4$-CNC is characterized using laser scanning confocal microscopy (LSCM). The luminescent domains appear to be homogeneous on the main surface and along the cross-section of the composite film (Fig. 1c, Inset, right and bottom bars). The uniform distribution of AuNC in the composite film is further confirmed by the energy dispersion X-ray (EDX) elemental mapping analysis (Fig. 1d, S3b). The distribution of AuNC is found uniform in the composite films of $AuNC_x$-CNC, where x is between 0.5 and 4 (Fig. S5, S6).

The composite films appear iridescence tinted with the light brown of AuNC (Fig. 2a). The tinted iridescence of $AuNC_x$-CNC becomes more intense with increasing AuNC loading, confirming the effective incorporation of AuNC into the chiral nematic structure of CNC. When viewed under 365 nm light, the composite films show red-emitting colours whose intensity increases with increasing AuNC loading (Fig. S7a). A redshift in reflectance wavelength of $AuNC_x$-CNC has been observed by the ultraviolet visible (UV-vis) spectroscopy alongside very intense peaks with positive ellipticity and redshifted peak positions by the circular dichroism (CD) spectra, indicating increased helical pitch (Fig. 2b, 2c). The CD spectra further confirm the left-handed chiral nematic order of the composite films. No additional CD signal is found, confirming that AuNC are achiral. POM images of the corresponding films show strong birefringence with the domain colour shifting from blue to green (Fig. S4). It appears that the stabilized distribution of AuNC in the composite film is determined and stabilized by the repulsive interactions between the negatively charged host and guest species when the volume of the AuNC solution is below 4.0 mL. Attempt to further increase AuNC loading results in a random aggregate of AuNC-CNC without chiral nematic ordering based on the SEM (Fig. S8).

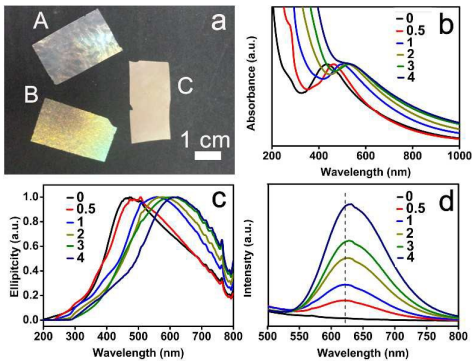

Fig. 2 Characterizing $AuNC_x$-CNC with varying AuNC loading. (a) Photograph of $AuNC_x$-CNC showing tunable iridescent colours (x = 0, 1, 4 for A, B and C, respectively). (b) UV-vis spectra, (c) CD spectra. (d) Fluorescence emission spectra showing that the peak position redshifts with increasing AuNC loading.

Notably, the fluorescent emission peak of the $AuNC_x$-CNC film redshifts from 622 nm of $AuNC_{0.5}$-CNC to 631 nm of $AuNC_4$- CNC with marked increase in peak intensity, showing concentration-dependent fluorescence (Fig. 2d). Increased AuNC loading appears to cause greater energy loss during the relaxation of excited electrons to ground state. Observation shows that $AuNC_4$-CNC emits an intense red fluorescence centred at 631 nm in contrast to 636 nm of the $AuNC_4$:CNC suspension and 640 nm of the AuNC solution under 365 nm light (Fig. S7b). The blueshift is likely associated with the space confinement and less dielectric environment of the chiral nematic host structure compared to AuNC in a solution environment.[16]

To further evaluate the fluorescence emission of the composite film, the relationship between the stopband peak wavelength and the fluorescence emission of $AuNC_x$-CNC was examined. $AuNC_x$-CNC composite films with different stopband positions were prepared by mixing AuNC with CNC suspension sonicated for a different period of time while fixing the ultrasound power. It is known that sonication may drive away trapped ions in the bound-water layer around CNC, resulting in a larger electrical double layer that weakens chiral interactions, leading to increased helical pitch and redshifted reflectance wavelength.[17] By using sonication treatment, three composite films of $AuNC_1$-CNC were prepared showing a progressive shift

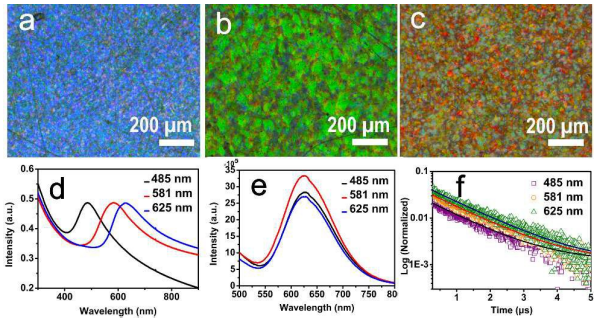

Fig. 3 Characterizing $AuNC_1$-CNC with the stopband positioned at 485 nm, 581 nm and 625 nm. (a)-(c): POM images showing a shift of domain colour from blue to red. (d) UV-vis spectra. (e) Fluorescence spectra (λex = 365 nm). (f) Room temperature fluorescence decay curves.

in the domain color from blue to red on the POM image with the peak wavelength of stopband of 485 nm, 581 nm and 625 nm, respectively, based on the UV-vis spectroscopy (Fig. 3a-3d). The corresponding CD spectra further confirm increased helical pitch (Fig. S9).

We discover that $AuNC_1$-CNC shows chiroptical-dependent fluorescence emission. As shown in Fig. 3e, the fluorescence intensity is in the order of $(AuNC_1\text{-}CNC)_{581}$ > $(AuNC_1\text{-}CNC)_{485}$ > $(AuNC_1\text{-}CNC)_{625}$. It is known that light with wavelength at the edge of stopband of a photonic crystal (band edge) propagates at reduced group velocity due to resonant Bragg scattering, leading to enhanced optical gain and stimulated photoemission with minimal losses. On the other hand, light with the wavelength close to photonic stopband cannot propagate through a photonic crystal. Considerable effort has been devoted to taking advantages of the stopband-and band edge-photoemission coupling effect for the design of ultrasensitive fluorescence sensors and high performance optical memory devices with fluorescence contrast (on/off ratio).[14a, 18] Chiral nematic liquid crystal is a one-dimensional photonic crystal, the enhancement and loss in the fluorescence intensity of $AuNC_1$-CNC at 581 nm and 625 nm are likely the manifestation of chiroptical-dependent spontaneous emission, given that the fluorescence emission of $AuNC_1$-CNC is centered at 623 nm (Fig. 2d). The fluorescence intensity of $AuNC_1$-CNC with the stopband at 485 nm is not affected as expected. The fluorescence lifetime decay of $AuNC_1$-CNC fits well to a biexponential decay model, $I(t) = A_1\exp(-t/\tau_1)+A_2\exp(-t/\tau_2)$, where τ_1 and τ_2 are the short and long decay time constants, and A_1 and A_2 are the contributions of respective decay component. The lifetime decay rate of $AuNC_1$-CNC with the stopband at 485 nm, 581 nm and 625 nm is in a decreasing order, showing the modulation of spontaneous emission by chiral nematic structure (Fig. 3f, Table S2).

We have demonstrated the ability of photonic CNC in modulating the spontaneous emission of AuNC through the photonic crystal-photoemission coupling effect. The amplification of fluorescent emission by chiral nematic structure offers a powerful and sustainable means for developing ultrasensitive optical devices with reduced detection limit and enhanced nonlinear response. AuNC have electron-rich surfaces due to the abundant amino groups of BSA. Studies show that electron-rich amine functionalized fluorescence donors show optical response in exposure to electron-deficient aromatic rings through charge transfer and electronic energy transfer mechanism causing fluorescence quenching.[19] To showcase the application potentials, a free-standing $AuNC_4$-CNC film was examined for nitroaromatic explosive sensing, for that, 2, 4, 6-trinitrophenol (TNP) was chosen as a model. Fingerprinting TNP solution on a free-standing $AuNC_4$-CNC film shows a clear fingerprint under 365 nm illumination and it becomes darker with increasing TNP concentration from 50 µM, 2 mM to 5 mM, qualifying $AuNC_4$-

CNC as a portable visual TNP sensor (Fig. 4a). The chiral nematic ordering of $AuNC_4$-CNC after exposure to TNP ethanol solution remains intact based on the SEM imaging analysis (Fig.

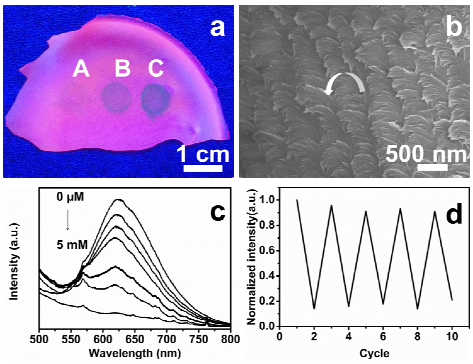

Fig. 4 Characterizing the sensing ability of $AuNC_4$-CNC for TNP. (a) Visual detection by fingerprinting using TNP solution as an ink. TNP concentration: 50 μM, 2 mM and 5 mM for A, B and C, respectively (λ_{ex} = 365 nm). (b) SEM image after the TNP test. (c) Fluorescence quenching spectra of $AuNC_4$-CNC film exposed to different TNP concentration (0， 10 μM，100 μM，500 μM, 1 mM，2 mM， 5 mM respectively). (d) The quenching and recovery test of $AuNC_4$-CNC film with five cycles.

4b). Further examination by immersing the $AuNC_4$-CNC sensor in TNP ethanol solution shows that the fluorescence intensity of the $AuNC_4$-CNC sensor decreases with increasing TNP concentration (Fig. 4c). The quenching and recovery tests of $AuNC_4$-CNC in ethanol solution show its performance stability and good recyclability (Fig. 4d).

We report that AuNC-CNC composite films show chiroptical- modulated fluorescent emission. The intensity of the fluorescence emission of AuNC-CNC can be enhanced through slow photon effect at the band-edge and suppressed by the photonic stopband. The chiroptical-modulated spontaneous emission is further manifested by the different rate of fluorescence lifetime decay. The observation of the chiroptical-dependent fluorescence emission reveals an important attribute of the chiral nematic materials that may lead to useful applications. More in-depth investigation is in progress to gain more insight into the modulation mechanism of the spontaneous emission by photonic cellulose nanocrystals.

Acknowledgements

Y. Xu is grateful to the financial support: NNSC (21171067 & 21373100), Jilin Provincial Talent Funds (802110000412) and Tang Aoqing Professor Funds of Jilin University (450091105161). C.F. Wu acknowledges financial support: “Thousand Young Talents Program” and NNSC (61222508 & 61335001).

Notes and references

1 (a) A. Bobrovsky, K. Mochalov, V. Oleinikov, A. Sukhanova, A. Prudnikau, M. Artemyev, V. Shibaev and I. Nabiev, *Adv. Mater.*, 2012, **24**, 6216-6222; (b) G. Muller, *Dalton. T.*, 2009, 9692-9707.
2 (a) S. Vignolini, P. J. Rudall, A. V. Rowland, A. Reed, E. Moyroud, R. B. Faden, J. J. Baumberg, B. J. Glover and U. Steiner, *Proc. Natl. Acad. Sci. USA.*, 2012, **109**, 15712-15715; (b) G. Strout, S. D. Russell, D. P. Pulsifer, S. Erten, A. Lakhtakia and D. W. Lee, *Annals of Botany*, 2013.
3 L. Wang and Q. Li, *Adv. Funct. Mater.*, 2015, n/a-n/a.
4 J. F. Revol, H. Bradford, J. Giasson, R. H. Marchessault and D. G. Gray, *Int. J. Biol. Macromol.*, 1992, **14**, 170-172.
5 (a) K. E. Shopsowitz, H. Qi, W. Y. Hamad and M. J. MacLachlan, *Nature*, 2010, **468**, 422-425; (b) K. E. Shopsowitz, W. Y. Hamad and M. J. MacLachlan, *J. Am. Chem. Soc.*, 2012, **134**, 867-870; (c) K. E. Shopsowitz, A. Stahl, W. Y. Hamad and M. J. MacLachlan, *Angew. Chem. Int. Ed.*, 2012, **51**, 6886-6890.
6 (a) G. Chu, J. Feng, Y. Wang, X. Zhang, Y. Xu and H. Zhang, *Dalton. T*, 2014, **43**, 15321-15327; (b) G. Chu, W. Xu, D. Qu, Y. Wang, H. Song and Y. Xu, *J. Mater. Chem. C.*, 2014, **2**, 9189-9195; (c) G. Chu, X. Wang, T. Chen, W. Xu, Y. Wang, H. Song and Y. Xu, *J. Mater. Chem. C.*, 2015, **3**, 3384-3390.
7 (a) H. Qi, K. E. Shopsowitz, W. Y. Hamad and M. J. MacLachlan, *J. Am. Chem. Soc.*, 2011, **133**, 3728-3731; (b) A. Querejeta Fernández, G. Chauve, M. Methot, J. Bouchard and E. Kumacheva, *J. Am. Chem. Soc.*, 2014, **136**, 4788-4793; (c) M. Schlesinger, M. Giese, L. K. Blusch, W. Y. Hamad and M. J. MacLachlan, *Chem. Commun.*, 2015, **51**, 530-533; (d) G. Chu, X. Wang, H. Yin, Y. Shi, H. Jiang, T. Chen, J. Gao, D. Qu, Y. Xu and D. Ding, *ACS. Appl. Mater. Inter.*, 2015, **7**, 21797-21806; (e) A. Querejeta Fernández, B. Kopera, K. S. Prado, A. Klinkova, M. Methot, G. Chauve, J. Bouchard, A. S. Helmy and E. Kumacheva, *ACS Nano*, 2015, **9**, 10377-10385.
8 G. Chu, X. Wang, T. Chen, J. Gao, F. Gai, Y. Wang and Y. Xu, *ACS. Appl. Mater. Inter.*, 2015, **7**, 11863-11870.
9 (a) H. Thérien Aubin, A. Lukach, N. Pitch and E. Kumacheva, *Angew. Chem.*, 2015, **127**, 5710-5714; (b) H. Therien Aubin, A. Lukach, N. Pitch and E. Kumacheva, *Nanoscale*, 2015, **7**, 6612-6618.
10 (a) T. D. Nguyen, W. Y. Hamad and M. J. MacLachlan, *Adv. Funct. Mater.*, 2014, **24**, 777-783; (b) S. H. M. Mehr, M. Giese, H. Qi, K. E. Shopsowitz, W. Y. Hamad and M. J. MacLachlan, *Langmuir*, 2013, **29**, 12579-12584.
11 L. Y. Chen, C. W. Wang, Z. Yuan and H. T. Chang, *Anal. Chem.*, 2015, **87**, 216-229.
12 J. Zheng, C. Zhang and R. M. Dickson, *Phys. Rev. Lett.*, 2004, **93**, 077402.
13 (a) J. Xie, Y. Zheng and J. Y. Ying, *J. Am. Chem. Soc.*, 2009, **131**, 888-889; (b) S. Yoon, E. W. Miller, Q. He, P. H. Do and C. J. Chang, *Angew. Chem. Int. Ed.*, 2007, **46**, 6658-6661; (c) C. H. Quek and K. W. Leong, *Nanomaterials*, 2012, **2**, 92-112.
14 (a) H. Li, J. Wang, H. Lin, L. Xu, W. Xu, R. Wang, Y. Song and D. Zhu, *Adv. Mater.*, 2010, **22**, 1237-1241; (b) N. Ganesh, W. Zhang, P. C. Mathias, E. Chow, J. A. N. T. Soares, V. Malyarchuk, A. D. Smith and B. T. Cunningham, *Nat Nano*, 2007, **2**, 515-520; (c) K. Min, S. Choi, Y. Choi and H. Jeon, *Nanoscale*, 2014, **6**, 14531-14537.
15 X. M. Dong, T. Kimura, J. F. Revol and D. G. Gray, *Langmuir*, 1996, **12**, 2076-2082.
16 C. L. Zhang, K. P. Lv, H. P. Cong and S. H. Yu, *Small*, 2012, **8**, 648-653.
17 S. Beck, J. Bouchard and R. Berry, *Biomacromolecules*, 2011, **12**, 167-172.
18 (a) M. Li, F. He, Q. Liao, J. Liu, L. Xu, L. Jiang, Y. Song, S. Wang and D. Zhu, *Angew. Chem.*, 2008, **120**, 7368-7372; (b) P. C. Mathias, N. Ganesh and B. T. Cunningham, *Anal. Chem.*, 2008, **80**, 9013-9020.
19 (a) Y. Ma, H. Li, S. Peng and L. Wang, *Anal. Chem.*, 2012, **84**, 8415-8421; (b) Y. Wang and Y. Ni, *Anal. Chem.*, 2014, **86**, 7463-7470.